Biodegradable Antimicrobial Agent/Analgesic/Bone Morphogenetic Protein-Loaded Nanofibrous Fixators for Bone Fracture Repair

Yi-Hsun Yu
Chang Gung Memorial Hospital Linkou Main Branch: Chang Gung Memorial Hospital
Yu-Ting Lin
Chang Gung University College of Engineering
Yung-Heng Hsu
Chang Gung Memorial Hospital Linkou Main Branch: Chang Gung Memorial Hospital
Ying-Chao Chou
Chang Gung Memorial Hospital Linkou Main Branch: Chang Gung Memorial Hospital
Wen-Neng W. N. Ueng
Chang Gung Memorial Hospital Linkou Main Branch: Chang Gung Memorial Hospital
Shih-Jung Liu (shihjung@mail.cgu.edu.tw)
Chang Gung University College of Engineering

Research

Keywords: sheath-core structured nanofiber, bone union, biodegradable fixator, antimicrobial, analgesics, growth factor

Posted Date: June 17th, 2021

DOI: https://doi.org/10.21203/rs.3.rs-608047/v1

Abstract

Background

Post-operative infection and pain management are two critical aspects that are of great concern to orthopedic surgeons. Although there are several protocols available to deal with these issues, they are fraught with complications such as cartilage damage, cardiovascular and neurological intoxication, and systemic adverse responses. Therefore, it is necessary to develop safe and effective perioperative protocols. In the present study, antimicrobial agents/analgesics/growth factor-embedded biodegradable hybrid fixators (polycaprolactone fixator + poly[lactide-co-glycolide] sheath-core structured nanofibers) for bone fracture repair were designed. These fixators were fabricated using solution-extrusion three-dimensional printing and electrospinning. The *in vitro* and *in vivo* release of the incorporated vancomycin, ceftazidime, lidocaine, and bone morphogenetic protein-2 (BMP-2) was evaluated. The *in vivo* efficacy of the biomolecule-loaded nanofibrous fixators was investigated in rabbit rib-fracture models.

Results

The nanofibrous fixators were shown to release vancomycin, ceftazidime, and lidocaine in a sustained manner in both *in vitro* and *in vivo* conditions and protected BMP-2 from burst release. The implantation of these hybrid fixators around the fractured rib significantly improved animal activities and bone union indicating that the inclusion of analgesic in the fixator effectively reduced the post-surgical pain and thereby helped in recovery.

Conclusions

The novel biomolecule-loaded nanofibrous hybrid fixators resulted in excellent therapeutic outcomes. They may be effective in the repair of rib fractures in clinical settings and may help deal with surgical complications such as infection, non-union, and intolerable post-operative pain.

1. Background

Technological advancements in medical sciences have accelerated developments in osteosynthesis models and devices. For example, the bone-healing process is no longer reliant on endogenous growth factors alone; instead, synthetic growth factors are added to the fracture site to facilitate fracture repair [1, 2]. In this case, although a high rate of bone union can be achieved, there are several factors that may cause non-union, including bone loss and defects, excessive periosteal damage during osteosynthesis, and locally colonized microorganisms [3–5]. Among these, microorganism colonization, also known as “infection,” before and after osteosynthesis is a dominant factor [6–8].

Surgeons are greatly concerned about perioperative infection, which may lead to missed surgical goals, impair the patient's functions, and cause complications, which may sometimes be fatal. In orthopedic surgeries, bone infection (i.e., osteomyelitis) may be the most troublesome complication of concern for orthopedic surgeons [9]. A non-union is generally observed after osteosynthesis in infected bones and requires long-term parenteral antimicrobial treatment and revision osteosynthesis with new bone transplantation. Thus, the addition of exogenous growth factors may be needed to achieve fracture union and regain normal function.

In contrast, patients undergoing orthopedic surgery are highly concerned about perioperative pain management. Pain is an important factor in recovery as it takes a significant physical and mental toll on the patient [10, 11]. To counter these problems, several pain management protocols have been proposed [12–14]. One of these protocols suggests soaking surgical tissues with analgesics [15–19]. Although this local bulk-absorption method is effective, it is accompanied by complications such as cartilage damage [20], cardiovascular intoxication, and impaired neurological response [21, 22]. Therefore, a safe and effective perioperative pain management protocol is essential.

To address these issues, we developed degradable nanofibrous fixators loaded with antimicrobial agents, analgesics, and growth factors for repairing bone fractures. The fixators were fabricated using three-dimensional (3D) printing and electrospinning/co-electrospinning. In our previous study [23], we employed micro-injection molding to prepare biodegradable fixators. Compared to injection molding, 3D printing enables faster and customized product development [24, 25]. The lead time for manufacturing can also be reduced substantially; thus the new designs have shorter time-to-market and can meet customer demands more quickly. Moreover, the electrospinning technique yields non-woven mats with a thickness on the order of a few nanometers with large surface areas, ease of functionalization, and superior mechanical properties [26, 27]. Further, the co-electrospinning technique can be used to prepare sheath-core structured nanofibers.

We selected poly(ε-caprolactone) (PCL), a popular long-term implantable biomaterial [23, 28, 29], as the backbone of the biodegradable fixators as it undergoes gradual degradation by the hydrolysis of ester linkages under normal physiological conditions (such as those in the human body). To prepare nanofibers, we chose poly (lactic-co-glycolic acid) (PLGA), which is a US Food and Drug Administration-approved copolymer often used in therapeutic devices owing to its excellent biodegradability and biocompatibility [30, 31].

In the current study, we aimed to evaluate the eluting profiles and clinical effectiveness of hybrid fixators with a PCL backbone and biomolecule (antimicrobial medication, analgesic agent, and growth factor)-embedded PLGA nanofibers in a rabbit rib-fracture model. We hypothesized that by implanting these hybrid fixators in the fracture models, bone union can be secured, and the loaded drugs will be eluted gradually resulting in efficient bone union and growth.

2. Results

2.1 Mechanical strength of degradable fixators

The load-displacement curves of the H2, H3, and X biodegradable fixators fabricated in this study are shown in Fig. 1. Thicker fixators (0.4 mm) showed significantly higher strengths than their thinner counterparts (0.2 mm). The experimental results also showed that X and H3 fixator-repaired ribs were stronger than those repaired with H2; however, the strength of the repaired ribs was still lower than that of control (unfractured) ribs. It should be noted that there were no statistical differences among the three fixators (H2 vs. H3, $p = 0.11$; H2 vs. X, $p = 0.06$; H3 vs. X, $p = 0.06$). Regarding the time required for fixation, H2 required the least amount of time (H2: 60 s; H3: 90 s; X: 180 s). Therefore, we selected the H2 fixator for subsequent *in vivo* studies.

2.2 Characterization of biomolecule-loaded nanofibers

The Scanning electron microscopy (SEM) images of pure PLGA, drug-loaded, and BMP-2-incorporated nanofibers are shown in Fig. 2A to C along with their size distributions. The diameter of pure PLGA nanofibers (577 ± 465 nm; Fig. 2A) was larger than that of drug-embedded PLGA nanofibers (131 ± 58 nm; Fig. 2B), and the coaxially electrospun BMP-2/PLGA nanofibers (2.85 ± 0.28 μm; Fig. 2C) exhibited the largest diameter. Figure 2D shows a Transmission electron microscopy (TEM) image of PLGA/BMP-2 nanofibers in which a sheath-core structure can be clearly observed.

The water contact angles of pure PLGA, drug-loaded, and sheath-core PLGA/BMP-2 nanofibers and PCL fixators were 128.1°, 79.2°, 121.5°, and 103.5°, respectively. Clearly, the addition of drugs to the nanofibers greatly increased their hydrophilicity.

FTIR spectra of pure PLGA and drug-loaded PLGA electrospun mats are shown in Fig. 3. The new vibration peak at 1676 cm^{-1} in the spectrum corresponding to drug-loaded PLGA is attributed to the C = C bonds of the aromatic rings in the drug molecules. The peak at 1762 cm^{-1} may be ascribed to the C = O bonds of incorporated drugs. The peak near 2996 cm^{-1}, corresponding to CH_2 bonds, was enhanced upon the addition of drugs to the nanofiber mat. Meanwhile, the absorption band observed at 3422 cm^{-1} in the FTIR spectrum of drug-loaded PLGA could be attributed to the N-H bonds of vancomycin, ceftazidime, and lidocaine. Thus, the obtained FTIR spectra demonstrate the successful incorporation of antimicrobial and analgesic agents in PLGA nanofibers.

2.3 *In vitro* and *in vivo* eluting profiles

The *in vitro* eluting profiles of drugs loaded in the PLGA nanofibers are shown in Fig. 4A and B. The results suggest that the drug-containing nanofibers released vancomycin and ceftazidime in a sustained manner at concentrations higher than their minimum inhibitory concentrations (MICs) for 30 and 24 days, respectively. Meanwhile, lidocaine was released for over 15 days. In all three cases, a high rate of elution was observed in the first 3 days, followed by gradual and continued elution, except that a second peak of drug release was found. The *in vitro* elution of BMP-2 from the nanofibers was also characterized. As

shown in Fig. 4C, the sheath-core structured nanofibers could sustainably release BMP-2 for more than 30 days in a fairly stable manner. This might be due to the fact that BMP-2 was embedded in the core part of the sheath-core nanofibers. In other words, the PLGA sheath exerted a shielding effect and protected BMP-2 from a burst release. The *in vivo* concentrations of drugs released in the animal models were also measured (Fig. 4D). It can be observed that the nanofibers released the drugs in an extended manner for more than 28 days. Additionally, although the drug concentrations in the tissues were high, drug levels in the blood remained low throughout the study period.

2.4 Efficacy of pain control of drug-loaded PLGA nanofibers in animal models

To determine the efficacy of the incorporated analgesics, animal activities were examined post-surgery. Figure 5A shows the numbers of lattice zones (1–9) of the animal bioactivity cage (ABC). The data in Fig. 5B shows that lattice zone 1 (diet) was the most inhabited in the control group, whereas lattice zone 7 (corner) was the most visited zone in the fixator/drugs group. Meanwhile, lattice zone 5 was the least inhabited zone in both groups. A comparison of daily activity counts (Fig. 5C) on each day between the fixator and fixator/drugs groups revealed significant differences ($p < 0.05$). Although there was no significant difference between the control and fixator/drugs groups, the 7-day counts indicated significant differences between the fixator and fixator/drugs groups ($p < 0.05$).

2.5 Gross and histological examinations

Gross and histological examinations of the target ribs treated with hybrid fixators were carried out (Fig. 6A to H). Gross examination revealed that the PLGA nanofibers were absorbed with the PCL-based rib fixators around the rib without breaking the locking mechanism. All fractures achieved union. CT scans of the ribs revealed a continuous and circumferential bridging callus in three out of four specimens. One specimen revealed incomplete union, representing cortical discontinuity (Fig. 6B). Histological examination of the tissue surrounding the hybrid fixators indicated rich mono- and multi-nucleated cells, along with a certain number of fibroblasts in the first 2 weeks, and a gradually decreasing tissue reaction by the 3rd and 4th weeks (Fig. 6E to H).

3. Discussion

In this study, we fabricated biomolecule (antibiotics, analgesics, and bone growth factor)-loaded nanofibrous biodegradable fixators using 3D printing and electrospinning/co-electrospinning for promoting bone union in osteosynthesis. The biodegradable fixators described herein could overcome the limitations posed by traditional metallic fixators, such as mechanical load mismatch, graft lacerations, secondary surgical removal, and hindrance during post-operative magnetic resonance imaging and CT scanning. Furthermore, the biomolecule-loaded degradable fixators delivered drugs and growth factors in a sustained manner to the target sites to enhance bone healing.

Perioperative infection during osteosynthesis is of great concern in orthopedic surgeries. Various prophylactic approaches to control bacterial colonization are used to help ensure clean orthopedic surgeries, including prolonged systemic antimicrobial medications, local antimicrobial solution rinse and irrigation, and local application of an antimicrobial powder [32–35]. However, each of these methods has its own limitations, such as a less-than-optimal infection prevention, reaction with local tissues, healing inhibition, and systemic toxicity. Therefore, we loaded antimicrobial medication in PLGA nanofibers to ensure a continuous supply of antibiotics to the surgical site. In our experiments, we noted that the concentration of the applied antimicrobial agents remained high, yet localized, without systemic spreading. Owing to these advantages, it is suggested that the hybrid fixator design described in the current study can not only be used during surgeries as an infection prophylaxis but also as a definite treatment for chronic osteomyelitis for complete eradication of microorganisms.

The treatment course described in this study can be especially helpful in cases of chronic osteomyelitis in fracture non-union (infective non-union), for both patients and surgeons. Although we did not conduct *in vivo* bactericidal assays, the PLGA nanofibers were loaded with two common antimicrobial medications, vancomycin, and ceftazidime, which can eradicate most Gram-positive and Gram-negative microorganisms encountered in osteomyelitis [36–38]. The hybrid fixator assembly described herein exhibited sustained elution of antimicrobial drugs at levels higher than their MIC for up to 28 days, thereby creating an environment in which infection could be effectively prevented and osteomyelitis treated. Additionally, the continuous elution of BMP-2 from PLGA nanofibers is expected to facilitate repair in non-union cases. As observed in our analyses, all fractures in the animal models were united within 28 days.

Another significant finding of our study is the analgesic effect provided by lidocaine eluted from multi-drug-loaded PLGA nanofibers. One of the biggest concerns of patients receiving medical treatment is pain, especially in orthopedic surgeries. Currently, there are several analgesic protocols available for application in the post-operative period [12–19]. However, inadequate pain control (via oral administration or parietal injection) and dangerous systemic side effects (from bulky absorption during intra-articular injection) are the drawbacks of these protocols. In this study, an analgesic was embedded in the biodegradable PLGA nanofibers, and its slow and continuous release is expected to greatly relieve post-operative pain. In our studies on the post-operative activities of rabbits that underwent surgery, we found that the animals implanted with analgesic-containing PLGA nanofibers were as active as those in the control group. In fact, the animals in the control and drug-loaded fixator groups were much more active than those in the fixator-only group (both in terms of daily activity and 7-day activity). This result demonstrates that the inclusion of analgesic in the fixator was effective in reducing post-surgical pain and, thus, helped recovery.

Although we endeavored to minimize any bias in our *in vitro* and *in vivo* analyses, there still remained some limitations. First, we did not create an infected animal model in which the bactericidal effect of the applied materials could have been evaluated during the study period. Second, the animal model used was not a non-union model; hence, the capacity of the hybrid fixator to facilitate bone union could be inferred

only from laboratory and image findings. Third, the post-operative behavior of the animals was evaluated only using an ABC. However, the strength of this study lies in the fact that the novel biomolecule-loaded nanofibrous fixator resulted in an excellent therapeutic outcome. Thus, these devices may be helpful in dealing with surgical complications such as infection, non-union, and intolerable post-operative pain.

4. Conclusions

In this study, we developed vancomycin, ceftazidime, lidocaine, and BMP-2-loaded biodegradable nanofibrous fixators based on PCL and PLGA for bone fracture repair. When tested on animal models, these biodegradable fixators ensured a sustained release of vancomycin, ceftazidime, and lidocaine for 30, 24, and 15 days, respectively, under *in vitro* conditions, and for 28 days (each compound) under *in vivo* conditions. In addition, the fixators released high concentrations of BMP-2 for more than 28 days and promoted bone union. Taken together, we successfully designed and developed a hybrid structure consisting of a PCL-based fixator and PLGA-based nanofibrous membranes loaded with antimicrobial agents, analgesics, and growth factors to promote bone union in fracture cases, aid in countering infections, and ameliorate post-operative pain.

5. Methods

5.1 Materials

The backbone of the fixators consisted of PCL (molecular weight [Mn] ~ 80,000 Da), and the drug carrier was PLGA, which consisted of a 1:1 ratio of lactide and glycolide and an Mn of 33,000 Da. The drugs used included commercial grade vancomycin hydrochloride, ceftazidime hydrate, and lidocaine hydrochloride. Recombinant human bone morphogenetic protein-2 (BMP-2) was used as the growth factor. The solvents used included dichloromethane (DCM) and 1,1,1,3,3,3-hexafluoro-2-propanol (HFIP). All these chemicals were purchased from Sigma-Aldrich (St. Louis, MO, USA).

5.2 Design and fabrication of biodegradable fixators

Three types of self-locking biodegradable fixators were designed (H2, H3, and X), as shown in Fig. 7A. The fixators were fabricated on a lab-developed solution-extrusion 3D printer [39], which included a solution-extrusion feeder, driving stepper motors and related components, power source, syringe controlled by a user interface, accumulation platform, and dispensing tip with an outlet inner diameter of 0.18 mm (Fig. 7B). An open Cura interface (Ultimaker B.V., Geldermalsen, The Netherlands) was used to manage the entire 3D printing procedure (Fig. 7C).

To print the fixators, 2.5 g of PCL was mixed with 3.5 mL of DCM on a magnetic stirrer for 6 h. The mixed solution was then fed into the feeding system of the printer, which consisted of a syringe and plastic dispensing tip. The dispensing tip was moved using a microprocessor-controlled servo motor during the 3D printing process, and the PCL solution was pushed out of the tip and deposited on the collection

platform. Upon solvent evaporation, biodegradable fixators of different geometrical designs and thicknesses (0.2 and 0.4 mm) were obtained.

5.3 Mechanical properties of the biodegradable fixators

A pilot *in vitro* study was initially conducted to assess the mechanical properties of the biodegradable fixators prior to *in vivo* animal studies. Four 6-month-old New Zealand white rabbits weighing 2800–3200 g were used in the biomechanical tests. Each rabbit was placed in an enclosed chamber, and inhalation euthanasia was carried out using carbon dioxide (2 L/min for 3 min). Carbon dioxide was pumped for an additional 2 min to ensure a complete lack of respiration and faded eye color. All animal procedures received institutional approval from the Institutional Animal Care and Use Committee at the Animal Center of Chang Gung University (CGU 14–102). Additionally, each rabbit was cared for in accordance with the regulations of the National Institutes of Health of Taiwan.

In total, 21 ribs were harvested (bilateral 5th to 7th ribs in each rabbit) and examined. The ribs were prepared by removing the attached muscles and periosteum after euthanasia. Each fixator was fixed to the ribs by passing belts through matching holes and wrapping around the fracture site; the time required for fixing was recorded. Subsequently, the control ribs and fixator–rib assemblies were analyzed using 3-point bending on a mechanical testing device (LRX, Lloyd Instruments, Bognor Regis, UK). The specimens were placed on two supporting pins 25 mm apart from each other, and the loading pin was moved at a speed of 1 mm/s in a downward direction until the specimen fractured. The applied force and strain in the ribs (control and fixator) during the loading process were recorded.

5.4 Fabrication of biomolecule-loaded nanofibers

Bilayered biomolecule-loaded nanofibers, i.e., a regular nanofibrous layer and a sheath-core structured layer, were prepared using electrospinning and co-electrospinning. An electrospinning setup, consisting of a high-voltage supply generating positive direct current voltage (maximal power: 35 kV) and current (4.16 mA/125 W), aluminum sheet, ground electrode, and syringe with a needle (0.4 mm internal diameter), was used to fabricate the regular nanofibers. To fabricate these nanofibers, PLGA (1120 mg), vancomycin hydrochloride (93.3 mg), ceftazidime hydrate (93.3 mg), and lidocaine hydrochloride (93.3 mg) were mixed with 5 mL of HFIP and used to fill the syringe pump. This solution was extruded from the syringe at a rate of 0.8 mL/h and electrospun on the aluminum sheet, which acted as the collector. The distance from the needle tip to ground electrode was 15 cm, and an 18 kV positive voltage was applied to the polymer solution.

Meanwhile, to fabricate the sheath-core structured nanofibers, a special coaxial device that concurrently deposited two solutions on the aluminum sheet was used [5]. PLGA (840 mg) was dissolved in 1 mL of HFIP and applied as the sheath solution, whereas the core solution consisted of 20 μg of BMP-2 and 1 μL of bovine serum albumin in 1 mL of phosphate-buffered saline (PBS). For coaxial electrospinning, the PLGA and core liquids were placed in two separate feeding tubes equipped with needles. During co-electrospinning, the liquids were conveyed and spun onto the aluminum sheet at a rate of 0.9 and 0.3 mL/h for the shell PLGA and core BMP-2 solutions, respectively, using two independently controlled

pumps. A 17 kV positive voltage was applied to the solutions, and the distance between the needle tip and ground electrode was maintained at 15 cm.

All electrospinning experiments were carried out at room temperature (25°C), and the manufactured nanofibrous membranes were heated in a vacuum oven at 40°C for 72 h to vaporize any remaining solvents.

5.5 SEM

The morphology of the electrospun nanofibers was evaluated using SEM (JSM7500F, Jeol, Tokyo, Japan). To enhance sample conductivity, before testing, the membrane samples were initially coated with a thin layer of gold. Fiber diameters were analyzed from 100 randomly selected fibers (n = 3) using ImageJ software (National Institutes of Health, Bethesda, MD, USA).

5.6 TEM

The structure of the sheath-core nanofibers was analyzed using TEM (JEM-2000EXII, Jeol); samples for TEM analysis were prepared by directly depositing the fibers onto copper grids.

5.7 Water contact angle

The hydrophilicity of the electrospun nanofibers was examined in terms of their water contact angles (First Ten Angstroms, Newark, CA, USA). Nanofibrous membrane samples (10 × 10 mm^2) were prepared, and distilled water was slowly dropped onto their surfaces; the contact angles between water droplets and the membranes (n = 3) were evaluated using a video monitor. The water contact angle of PCL fixators was also measured for comparison.

5.8 Fourier-transform infrared (FTIR) spectroscopy

To analyze the functional groups present in the synthesized samples, the FTIR spectra of pure PLGA and drug-embedded PLGA nanofibers (in the form of pressed KBr disks) were recorded on a Nicolet iS5 spectrometer (Thermo Fisher Scientific, Waltham, MA, USA) at a resolution of 4 cm^{-1} over 32 scans in the wavenumber range of 400–4000 cm^{-1}.

5.9 *In vitro* release of pharmaceuticals and BMP-2

An *in vitro* elution method was employed to characterize the release patterns of vancomycin, ceftazidime, lidocaine, and BMP-2 from biomolecule-loaded PLGA nanofibers. Nanofiber samples (2 × 3 cm^2, 216–220 mg) were cut from the electrospun membranes and incubated in 1 mL of a PBS dissolution medium (0.15 mol/L, pH 7.4) at 37°C for 24 h. Subsequently, the dissolution medium was isolated and analyzed at 24 h intervals. PBS (1 mL) was replaced every 24 h until the sample was fully dissolved. Drug concentrations in the eluents were evaluated using a Hitachi L-2200R multisolvent delivery system (Tokyo, Japan), whereas the BMP-2 levels were analyzed using enzyme-linked immunosorbent assay (R&D Systems, Inc., Minneapolis, MN, USA).

5.10 Rib-fracture model

Twelve 6-month-old New Zealand male rabbits weighing 3.0 ± 0.2 kg were used for *in vivo* experiments. The right 6th rib was selected as the target rib. Each rabbit was anesthetized by inhalation of isoflurane after pre-oxygenation for 5 min, and the anesthetic was circulated throughout the experimental process. After administering the anesthetic, each rabbit was placed in the decubitus position with the surgical field upward. The skin was prepared and disinfected according to standard antiseptic procedures. A 3 cm incision was made along the rib, and the target rib was reached after dissecting the soft tissue layer and leaving the periosteum undamaged; a short oblique osteotomy was performed on each rib. These rabbits were then randomly divided into control, fixator, and fixator/drug groups (n = 4 per group). No osteosynthesis was performed in the control group, whereas in the remaining two groups, the osteotomized ribs were fixed either with the fixator alone or with the selected fixator accompanied by biomolecule-loaded PLGA nanofibers, which were circumferentially wrapped around the target rib (Fig. 8). Following the surgical procedure, the wound was repaired in layers with absorbable sutures. Post-operatively, the surgical wound was smeared with an antibiotic ointment, and the rabbits were returned to their cages after complete recovery from anesthesia and surgery.

5.11 *In vivo* release of drugs and BMP-2 from the electrospun nanofibers

To evaluate the local release and systemic diffusion of antimicrobial agents, analgesic, and growth factors embedded in PLGA nanofibers, the blood and muscle tissue surrounding the implanted PLGA nanofibers were obtained at regular intervals (post-operative days 2, 7, 14, and 28). After anesthetizing the rabbits, as described in Sect. 5.10, 1 mL of blood was extracted from the central auricular artery in their ears. Meanwhile, muscle tissue was obtained through the same skin incision on the operated chest wall. Both samples were preserved in 10% formalin solution and later analyzed using high-performance liquid chromatography (Hitachi L-2200 Multisolvent Delivery System).

5.12 Animal bioactivity

We assembled an ABC (30 × 30 × 30 cm^3) and divided it into nine lattice zones (numbered 1–9). Rabbit movement in these lattice zones was spontaneously detected using electric sensors placed above each lattice and connected to a recording computer. Food and water were supplied in lattice 1 and refilled every 24 h. The rabbits were sent to this designed cage after recovering from anesthesia and surgery for a 7-day observation and pain evaluation period.

During the evaluation process, each ABC was placed in an isolated room without people walking around, and constant temperature (21 °C ~ 24 °C), pressure (1 atmospheric pressure), and humidity (45%~70%) were maintained. Evaluation was completed after a 7-day bioactivity-evaluation course, after which the rabbits were sent to regular cages for routine care.

5.13 Microcomputed tomography (micro CT) and histology evaluation

Micro CT images (nanoScan SPECT/CT, Mediso, Hungary) were acquired to monitor the healing of fractured ribs in the fixator/drugs group. The osteotomized rib specimens were excised from rabbits euthanized 28 days after osteosynthesis. The specimens were sent for histological examination after hematoxylin and eosin staining.

5.14 Statistical analyses

All statistical data were processed using SPSS software (V17.0 for Windows; SPSS Inc, Chicago, IL, USA). Descriptive statistics are displayed as mean ± standard deviation. One-way analysis of variance (ANOVA) was conducted for data analysis and calculating statistical differences. The post-hoc Bonferroni method was used to compare pairs of groups to identify significant differences. The observed differences were considered statistically significant at $p < 0.05$.

Abbreviations

ABC, animal bioactivity cage; BMP-2, bone morphogenetic protein-2; 3D, three-dimensional; DCM, dichloromethane; FTIR, Fourier-transform infrared; HFIP, 1,1,1,3,3,3-hexafluoro-2-propanol; micro CT, microcomputed tomography; MIC, minimum inhibitory concentration; Mn, molecular weight; PBS, phosphate-buffered saline; PCL, poly(ε-caprolactone); PLGA, poly(lactic-co-glycolic acid); SEM, scanning electron microscopy; TEM, transmission electron microscopy.

Declarations

Ethics approval and consent to participate

The study protocol was approved by the Institutional Animal Care and Use Committee at the Animal Center of Chang Gung University (CGU 14-102).

Consent for publication

Not applicable

Availability of data and materials

All data generated or analyzed during this study are included in this published article.

Competing interests

The authors declare that they have no competing interests.

Funding

This work was supported by the Ministry of Science and Technology, Taiwan [grant number 109-2221-E-182-058-MY2]; and the Chang Gung Memorial Hospital [grant number CRRPD2K0011 and CRRPD2K0021].

Authors' contributions

Conception of the work: YH and SJ; Biomaterial synthesis and physicochemical characterization: YT, YH, and YC; biological studies: YH and YT; article preparation: YH, SWN, and SJ; all authors have approved the submitted version and have agreed both to be personally accountable for the author's own contributions and to ensure that questions related to the accuracy or integrity of any part of the work. All authors read and approved the fnal manuscript.

Acknowledgments

The authors thank the technical support of the molecular imaging facilities of the Laboratory Animal Center, Chang Gung Memorial Hospital-Linkou.

Authors' information (optional)

[a]Department of Orthopedic Surgery, Bone and Joint Research Center, Chang Gung Memorial Hospital, Tao-Yuan 33305, Taiwan

[b]Department of Mechanical Engineering, Chang Gung University, Tao-Yuan 33302, Taiwan

References

1. Schmidmaier G, Wildemann B, Ostapowicz D, Kandziora F, Stange R, Haas NP, et al. Long-term effects of local growth factor (IGF-I and TGF-beta 1) treatment on fracture healing. A safety study for using growth factors. J Orthop Res. 2004;22(3):514–9. doi:10.1016/j.orthres.2003.09.009.
2. Dumic-Cule I, Peric M, Kucko L, Grgurevic L, Pecina M, Vukicevic S. Bone morphogenetic proteins in fracture repair. Int Orthop. 2018;42(11):2619–26. doi:10.1007/s00264-018-4153-y.
3. Bell A, Templeman D, Weinlein JC. Weinlein. Nonunion of the femur and tibia: an update. Orthop Clin. 2016;47(2):365–75. doi:10.1016/j.ocl.2015.09.010.
4. Ross KA, O'Halloran K, Castillo RC, Coale M, Fowler J, Nascone JW, et al. Prediction of tibial nonunion at the 6-week time point. Injury. 2018;49(11):2075–82. doi:10.1016/j.injury.2018.07.033.
5. Tian R, Zheng F, Zhao W, Zhang Y, Yuan J, Zhang B, et al. Prevalence and influencing factors of nonunion in patients with tibial fracture: systematic review and meta-analysis. J Orthop Surg Res. 2020;15(1):377. doi:10.1186/s13018-020-01904-2.
6. Willey M, Karam M. Impact of infection on fracture fixation. Orthop Clin. 2016;47(2):357–64. doi:10.1016/j.ocl.2015.09.004.

7. Raven TF, Moghaddam A, Ermisch C, Westhauser F, Heller R, Bruckner T, et al. Use of Masquelet technique in treatment of septic and atrophic fracture nonunion. Injury. 2019;50(Suppl 3):40–54. doi:10.1016/j.injury.2019.06.018.
8. Zura R, Mehta S, Della Rocca GJ, Steen RG. Biological risk factors for nonunion of bone fracture. JBJS Rev. 2016;4(1):e5. doi:org/10.2106/jbjs.rvw.o.00008.
9. Metsemakers WJ, Kortram K, Morgenstern M, Moriarty TF, Meex I, Kuehl R, et al. Definition of infection after fracture fixation: a systematic review of randomized controlled trials to evaluate current practice. Injury. 2018;49(3):497–504. doi:10.1016/j.injury.2017.02.010.
10. Pitimana-aree S, Visalyaputra S, Komoltri C, Muangman S, Tiviraj S, Puangchan S, et al. An economic evaluation of bupivacaine plus fentanyl versus ropivacaine alone for patient-controlled epidural analgesia after total-knee replacement procedure: a double-blinded randomized study. Reg Anesth Pain Med. 2005;30:446–51. doi:10.1016/j.rapm.2005.05.010.
11. Zaslansky R, Eisenberg E, Peskin B, Sprecher E, Reis DN, Zinman C, et al. Early administration of oral morphine to orthopedic patients after surgery. J Opioid Manag. 2006;2:88–92. doi:10.5055/jom.2006.0014.
12. Wyatt MC, Wright T, Locker J, Stout K, Chappie C, Theis JC. Femoral nerve infusion after primary total knee arthroplasty: a prospective, double-blind, randomised and placebo-controlled trial. Bone Joint Res. 2015;4(2):11–6. doi:10.1302/2046-3758.42.2000329.
13. Olive DJ, Barriton MJ, Simone SA, Klufer R. A randomised controlled trial comparing three analgesia regimens following total knee joint replacement: continuous femoral nerve block, intrathecal morphine or both. Anaesth Intensive Care. 2015;43(4):454–60. doi: 10.1177%2F0310057X1504300406.
14. Peterson JR, Steele JR, Wellman SS, Lachiewicz PF. Surgeon-performed high-dose bupivacaine periarticular injection with intra-articular saphenous nerve block is not inferior to adductor canal block in total knee arthroplasty. J Arthroplasty. 2020;35(5):1233–8. doi:10.1016/j.arth.2020.01.030.
15. Chen DW, Hu CC, Chang YH, Lee MS, Chang CJ, Hsieh PH. Intra-articular bupivacaine reduces postoperative pain and meperidine use after total hip arthroplasty: a randomized, double-blind study. J Arthroplasty. 2014;29:2457–61. doi:10.1016/j.arth.2013.12.021.
16. Kendall MC, Alves LJC, De Oliveira G Jr. Liposome bupivacaine compared to plain local anesthetics to reduce postsurgical pain: an updated meta-analysis of randomized controlled trials. Pain Res Treat. 2018;2018:5710169. doi:10.1155/2018/5710169.
17. Berend ME, Berend KR, Lombardi AV Jr. Advances in pain management: game changers in knee arthroplasty. Bone Joint J. 2014;96-B:7–9. doi:10.1302/0301-620X.96B11.34514.
18. Hyland SJ, Deliberato DG, Fada RA, Romanelli RA, Collins CL, Wasielewski RC. Liposomal bupivacaine versus standard periarticular injection in total knee arthroplasty with regional anesthesia: a prospective randomized controlled trial. J Arthroplasty. 2019;34(3):488–94. doi:10.1016/j.arth.2018.11.026.

19. Ali A, Sundberg M, Hansson U, Malmvik J, Flivik G. Doubtful effect of continuous intraarticular analgesia after total knee arthroplasty: a randomized double-blind study of 200 patients. Acta Orthop. 2015;86:373–7. doi:10.3109/17453674.2014.991629.
20. Buchko JZ, Gurney-Dunlop T, Shin JJ. Knee chondrolysis by infusion of bupivacaine with epinephrine through an intra-articular pain pump catheter after arthroscopic ACL reconstruction. Am J Sports Med. 2015;43(2):337–44. doi: 10.1177%2F0363546514555667.
21. Sekimoto K, Tobe M, Saito S. Local anesthetic toxicity: acute and chronic management. Acute Med Surg. 2017;4(2):152–60. doi:10.1002/ams2.265.
22. Ballieul RJ, Jacobs TF, Herregods S, Van Sint Jan P, Wyler B, Vereecke H, et al. The peri-operative use of intra-articular local anesthetics: a review. Acta Anaesthesiol Belg. 2009;60(2):101–8.
23. Yu YH, Fan CL, Hsu YH, Chou YC, Ueng SWN, Liu SJ. A novel biodegradable polycaprolactone fixator for osteosynthesis surgery of rib fracture: in vitro and in vivo study. Materials. 2015;8(11):7714–22. doi:10.3390/ma8115415.
24. Kotta S, Nair A, Alsabeelah N. Alsabeelah. 3D printing technology in drug delivery: recent progress and application. Curr Pharm Des. 2018;24(42):5039–48. doi:10.2174/1381612825666181206123828.
25. Attaran M. The rise of 3-D printing: the advantages of additive manufacturing over traditional manufacturing. Bus Horiz. 2017;60(5):677–88. doi:10.1016/j.bushor.2017.05.011.
26. Hokmabad VR, Davaran S, Ramazani A, Salehi R. Design and fabrication of porous biodegradable scaffolds: a strategy for tissue engineering. J Biomater Sci Polym Ed. 2017;28(16):1797–825. doi:10.1080/09205063.2017.1354674.
27. Agarwal S, Wendorff JH, Greiner A. Use of electrospinning technique for biomedical applications. Polymer. 2008;49(26):5603–21. doi:10.1016/j.polymer.2008.09.014.
28. Kim J, Kudisch M, Mudumba S, Asada H, Aya-Shibuya E, Bhisitkul RB, et al. Biocompatibility and pharmacokinetic analysis of an intracameral polycaprolactone drug delivery implant for glaucoma. Invest Ophthalmol Vis Sci. 2016;57(10):4341–6. doi:10.1167/iovs.16-19585.
29. Chou YC, Cheng YS, Hsu YH, Yu YH, Liu SJ. Biodegradable nanofiber-membrane for sustainable release of lidocaine at the femoral fracture site as a periosteal block: In vitro and in vivo studies in a rabbit model. Colloids Surf B Biointerfaces. 2016;140:332–41. doi:10.1016/j.colsurfb.2016.01.011.
30. Yu YH, Hsu YH, Chou YC, Fan CL, Ueng SW, Kau YC, et al. Sustained relief of pain from osteosynthesis surgery of rib fracture by using biodegradable lidocaine-eluting nanofibrous membranes. Nanomedicine. 2016;12(7):1785–93. doi:10.1016/j.nano.2016.04.015.
31. Yu YH, Lee D, Hsu YH, Chou YC, Ueng SW, Chen CK, et al. A three-dimensional printed polycaprolactone scaffold combined with co-axially electrospun vancomycin/ceftazidime/bone morphological protein-2 sheath-core nanofibers for the repair of segmental bone defects during the Masquelet procedure. Int J Nanomedicine. 2020;15:913–25; doi: 10.2147%2FIJN.S238478.
32. Conterno LO, Turchi MD. Antibiotics for treating chronic osteomyelitis in adults. Cochrane Database Syst Rev. 2013;(9):CD004439; doi:10.1002/14651858.CD004439.pub3.

33. Dudareva M, Kümin M, Vach W, Kaier K, Ferguson J, McNally M, et al. Short or long antibiotic regimes in orthopaedics (SOLARIO): a randomised controlled open-label non-inferiority trial of duration of systemic antibiotics in adults with orthopaedic infection treated operatively with local antibiotic therapy. Trials. 2019;20(1):693. doi:10.1186/s13063-019-3832-3.
34. Cancienne JM, Burrus MT, Weiss DB, Yarboro SR. Applications of local antibiotics in orthopedic trauma. Orthop Clin North Am. 2015;46(4):495–510. doi:10.1016/j.ocl.2015.06.010.
35. Hake ME, Young H, Hak DJ, Stahel PF, Hammerberg EM, Mauffrey C. Local antibiotic therapy strategies in orthopaedic trauma: practical tips and tricks and review of the literature. Injury. 2015;46(8):1447–56. doi:10.1016/j.injury.2015.05.008.
36. Inzana JA, Schwarz EM, Kates SL, Awad HA. Biomaterials approaches to treating implant-associated osteomyelitis. Biomaterials. 2016;81:58–71. doi:10.1016/j.biomaterials.2015.12.012.
37. Hsu YH, Hu CC, Hsieh PH, Shih HN, Ueng SW, Chang Y. Vancomycin and ceftazidime in bone cement as a potentially effective treatment for knee periprosthetic joint infection. J Bone Joint Surg Am. 2017;99(3):223–31. doi:10.2106/JBJS.16.00290.
38. Hsu YH, Chen DW, Tai CD, Chou YC, Liu SJ, Ueng SW, et al. Biodegradable drug-eluting nanofiber-enveloped implants for sustained release of high bactericidal concentrations of vancomycin and ceftazidime: in vitro and in vivo studies. Int J Nanomedicine. 2014;9:4347–55. doi:10.2147/IJN.S66526.
39. Chen JM, Lee D, Yang JW, Lin SH, Lin YT, Liu SJ. Solution-extrusion additive manufacturing of biodegradable polycaprolactone. Appl Sci. 2020;10:3189. doi:10.3390/app10093189.

Figures

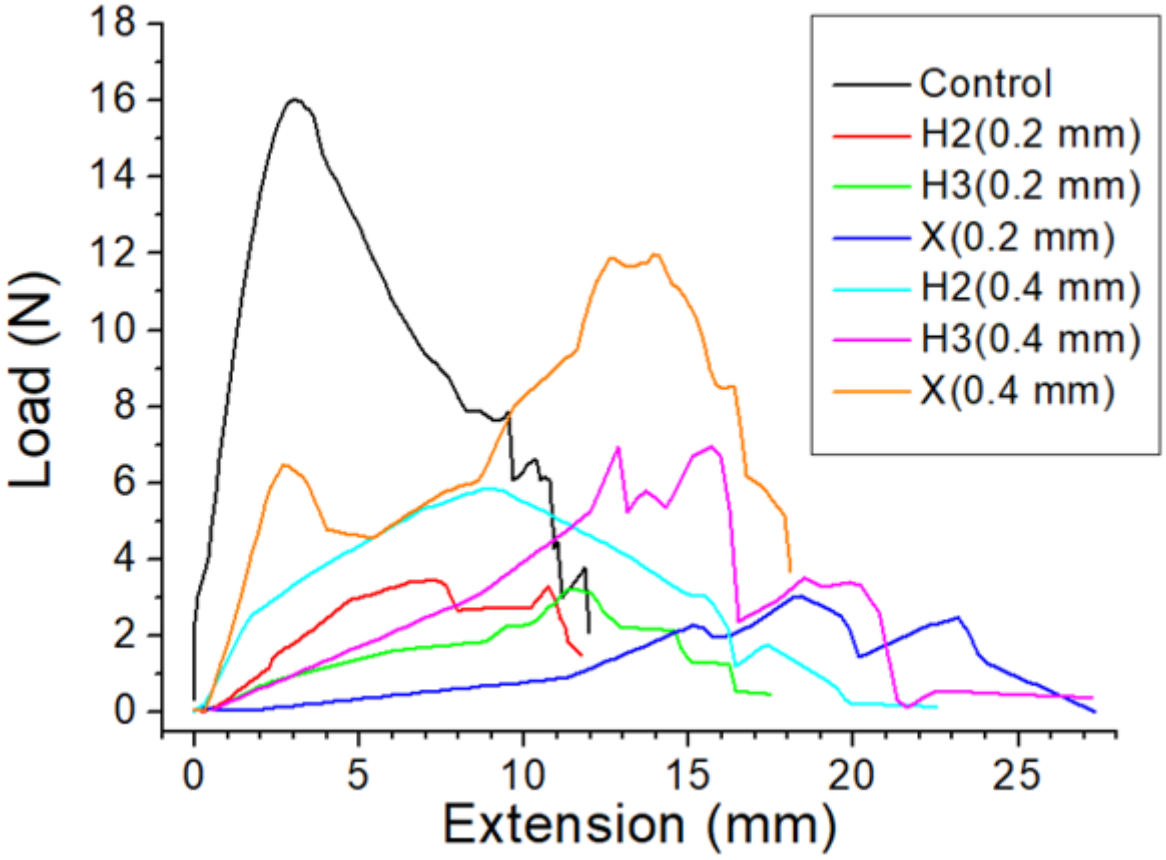

Figure 1

Representative tensile properties of the biodegradable fixators (control represents unfractured ribs).

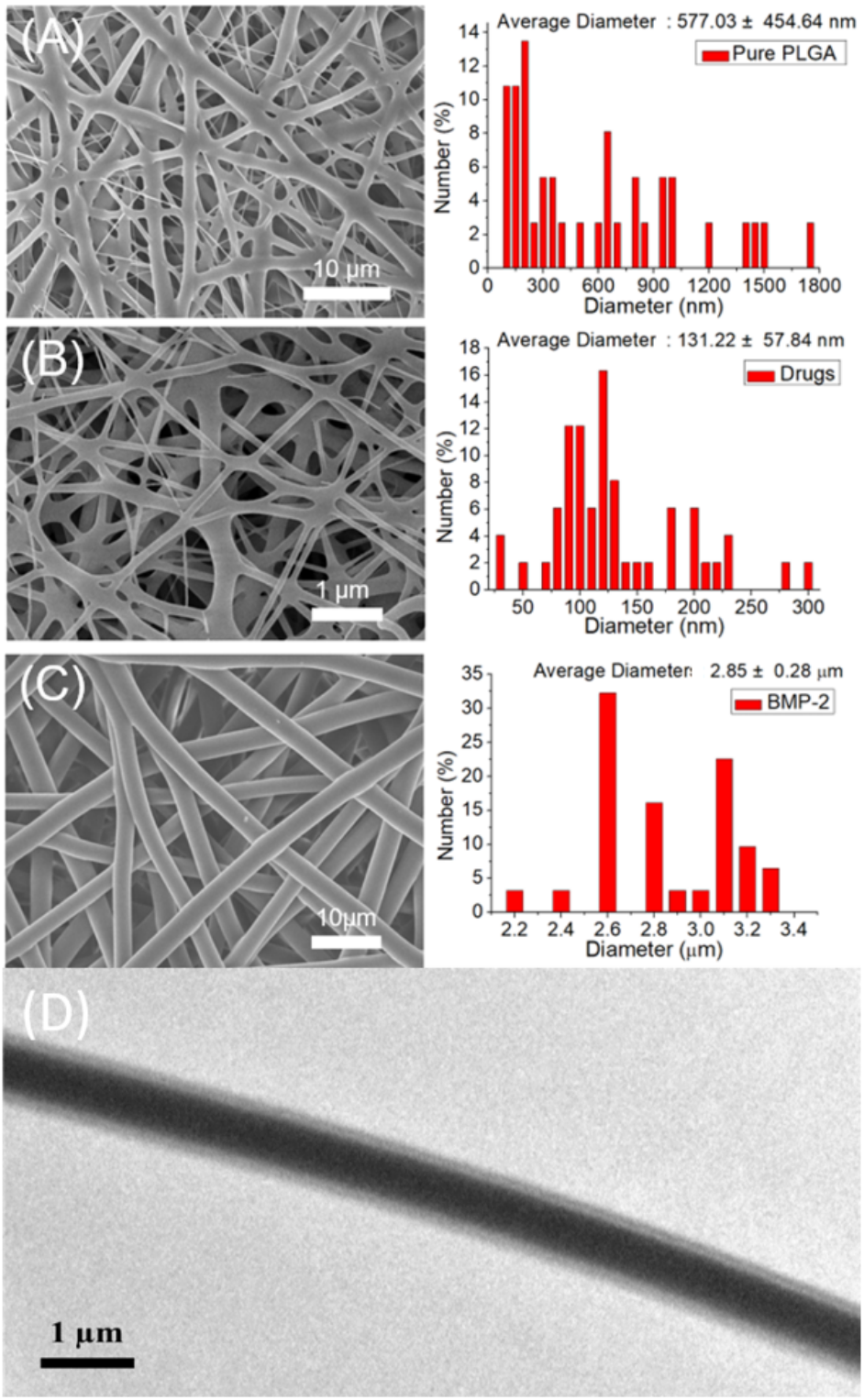

Figure 2

Scanning electron microscopy images of pure and biomolecule-loaded poly(lactic-co-glycolic acid) (PLGA) nanofibers and their size distributions. (A) Pure PLGA nanofibers, (B) drug-loaded nanofibers, and (C) bone morphogenetic protein-2 (BMP-2)-incorporated sheath-core structured nanofibers. (D) Transmission electron microscopy image of BMP-2-incorporated sheath-core structured nanofibers.

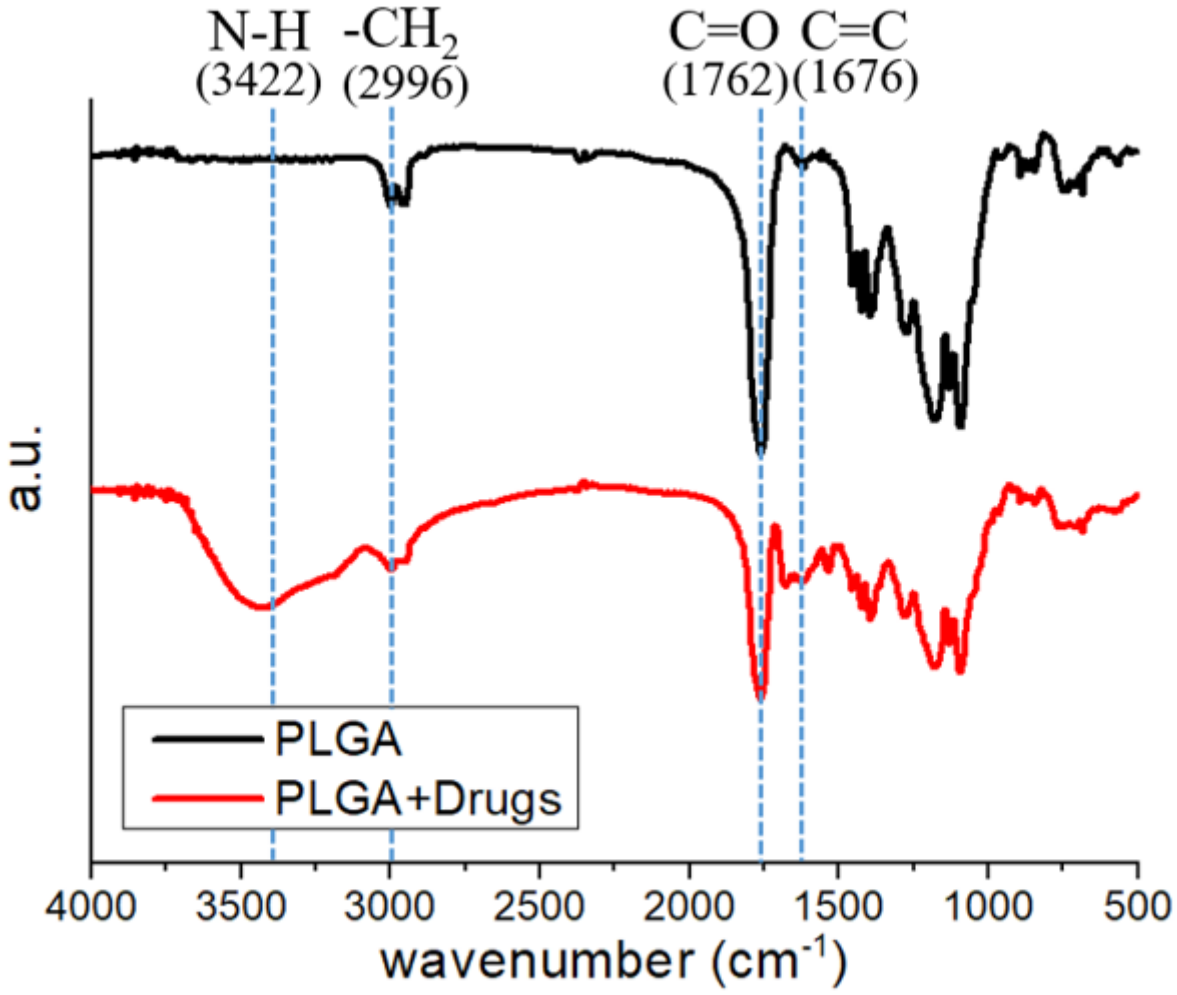

Figure 3

Fourier-transform infrared spectroscopy spectra of pure and drug-loaded poly(lactic-co-glycolic acid) (PLGA) nanofibers.

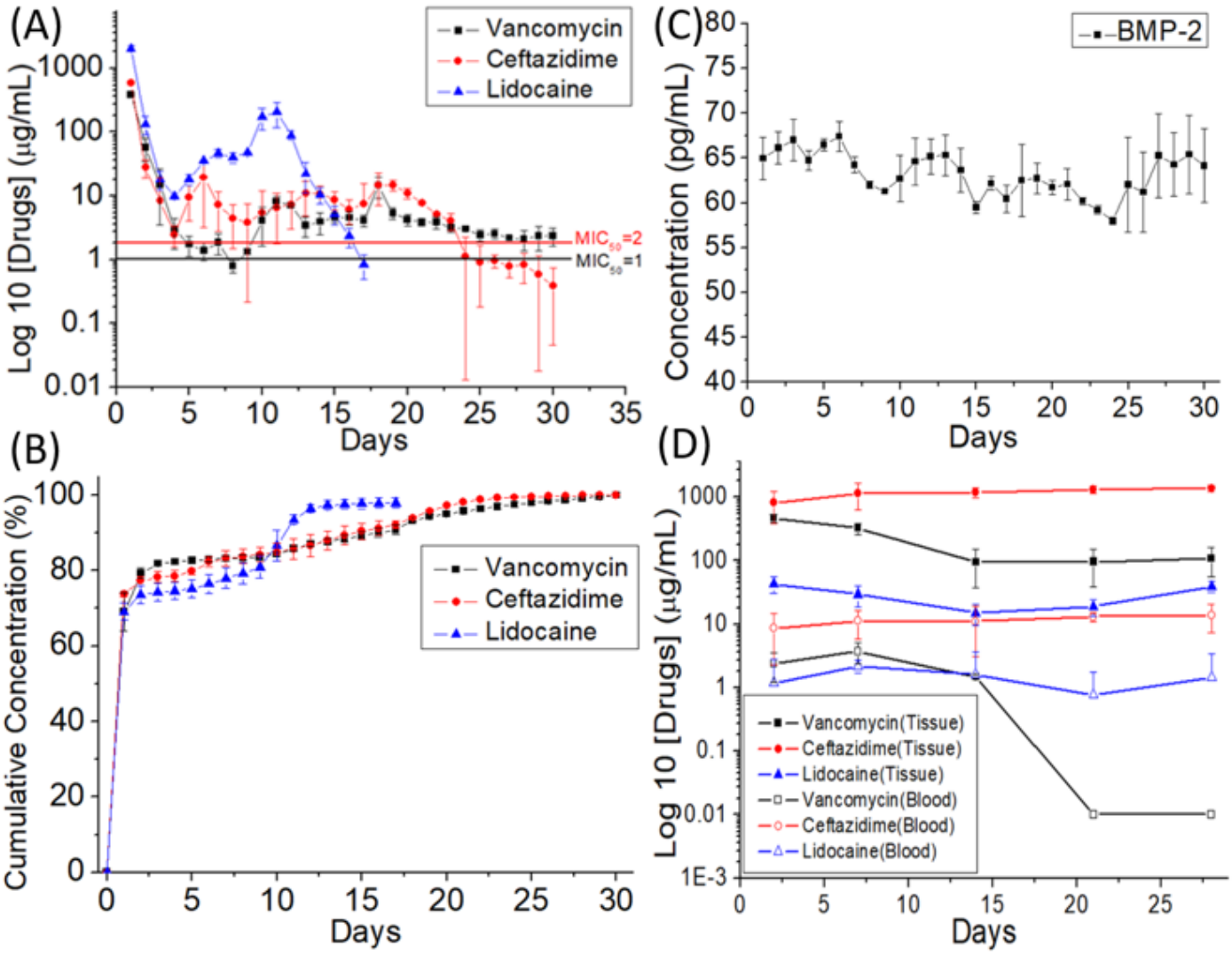

Figure 4

In vitro release profiles of carried pharmaceuticals (A to C). (A) Daily and (B) cumulative release of vancomycin, ceftazidime, and lidocaine from poly(lactic-co-glycolic acid) (PLGA) nanofibers. (C) Bone morphogenetic protein-2 (BMP-2) released from PLGA sheath-core nanofibers. (D) In vivo drug release from PLGA nanofibers in tissue and blood. Values represent the mean ± standard deviation (n =12).

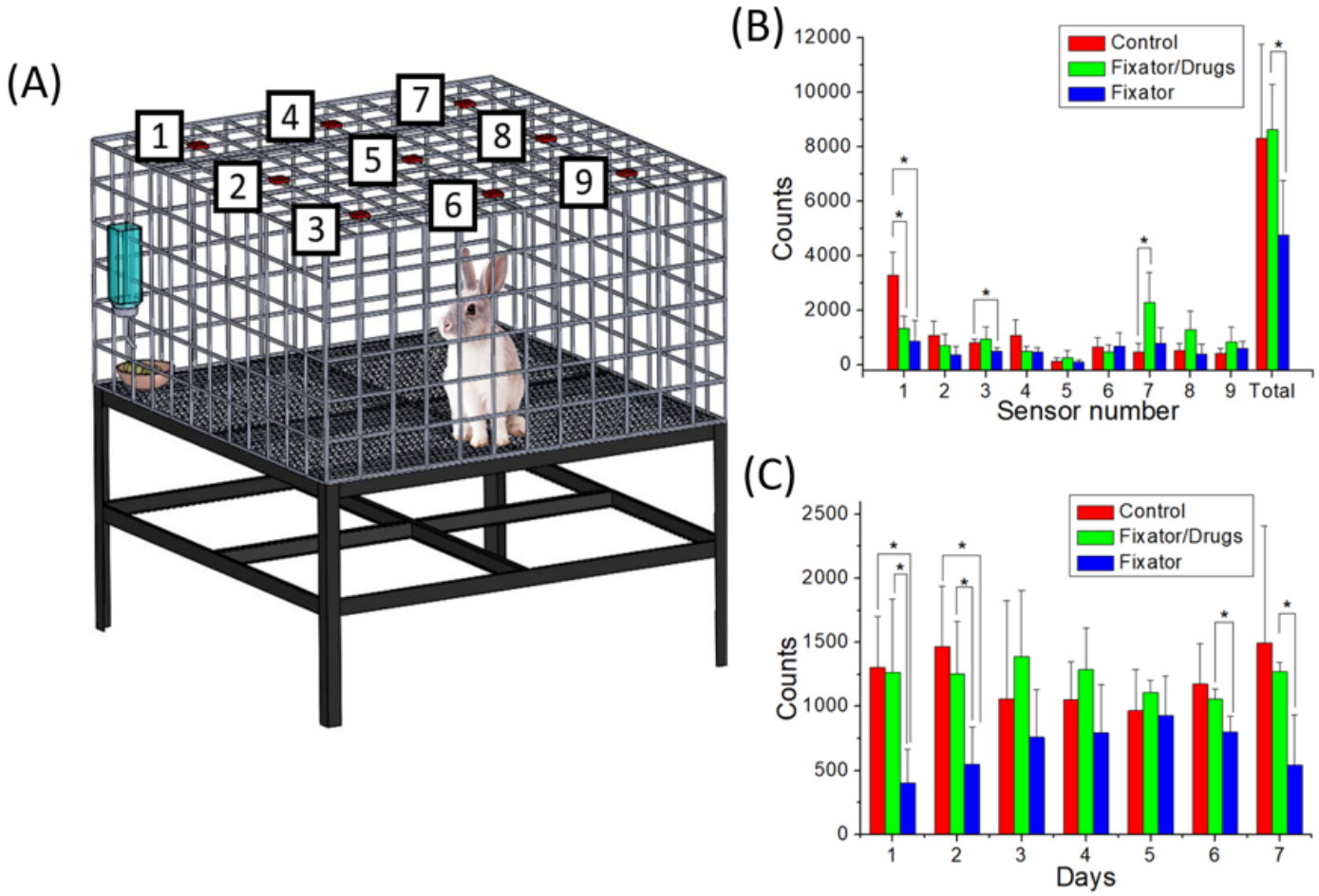

Figure 5

Schematic of an animal bioactivity cage (ABC). (A)Nine different lattice zones contained in the ABC for post-surgery evaluation. Animal activity counts in (B) each ABC lattice zones (sensor number) and (C) on different days for a total of 7 days. Values represent the mean ± standard deviation (n = 12); *p < 0.05.

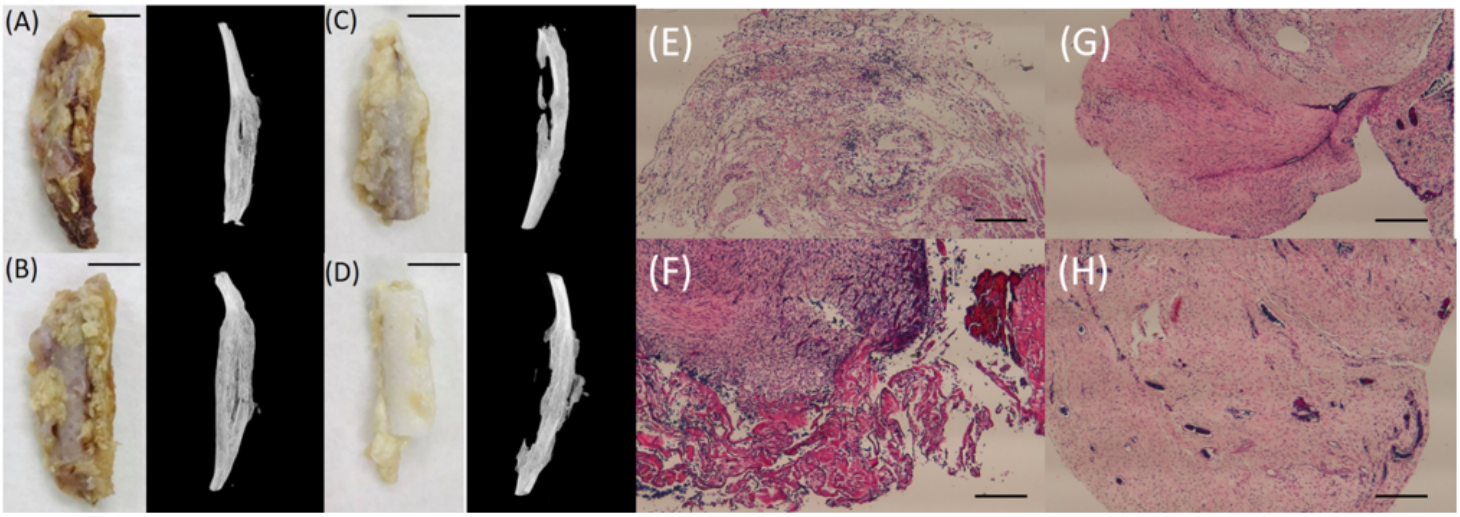

Figure 6

Clinical, radiological, and histological results of the animal study. (A-D) Experimental specimens (rib-fixator composites) and corresponding three-dimensional microcomputed tomography images of the fixator/drugs group. Scale bars, 1 cm. (E-H) Histological images (hematoxylin and eosin staining) of the fixator/drugs group at (E) one week, (F) two weeks, (G) three weeks, and (H) four weeks post-implantation. Scale bars, 500 μm.

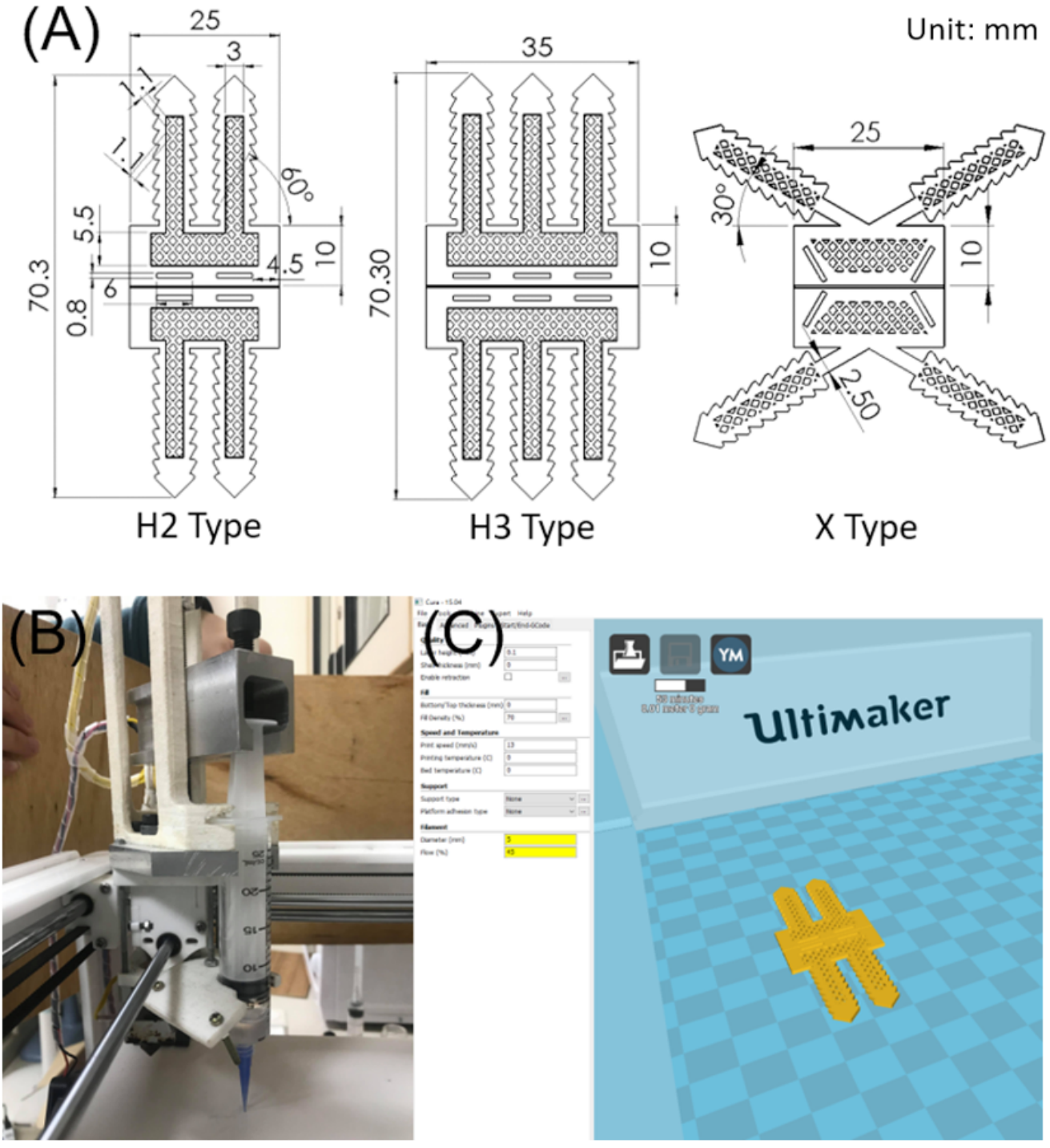

Figure 7

Fabrication process of 3D printing process. (A) Layouts and dimensions of the biodegradable fixators. (B) Photograph of the solution-extrusion 3D printer. (C) Cura code used to print the fixators.

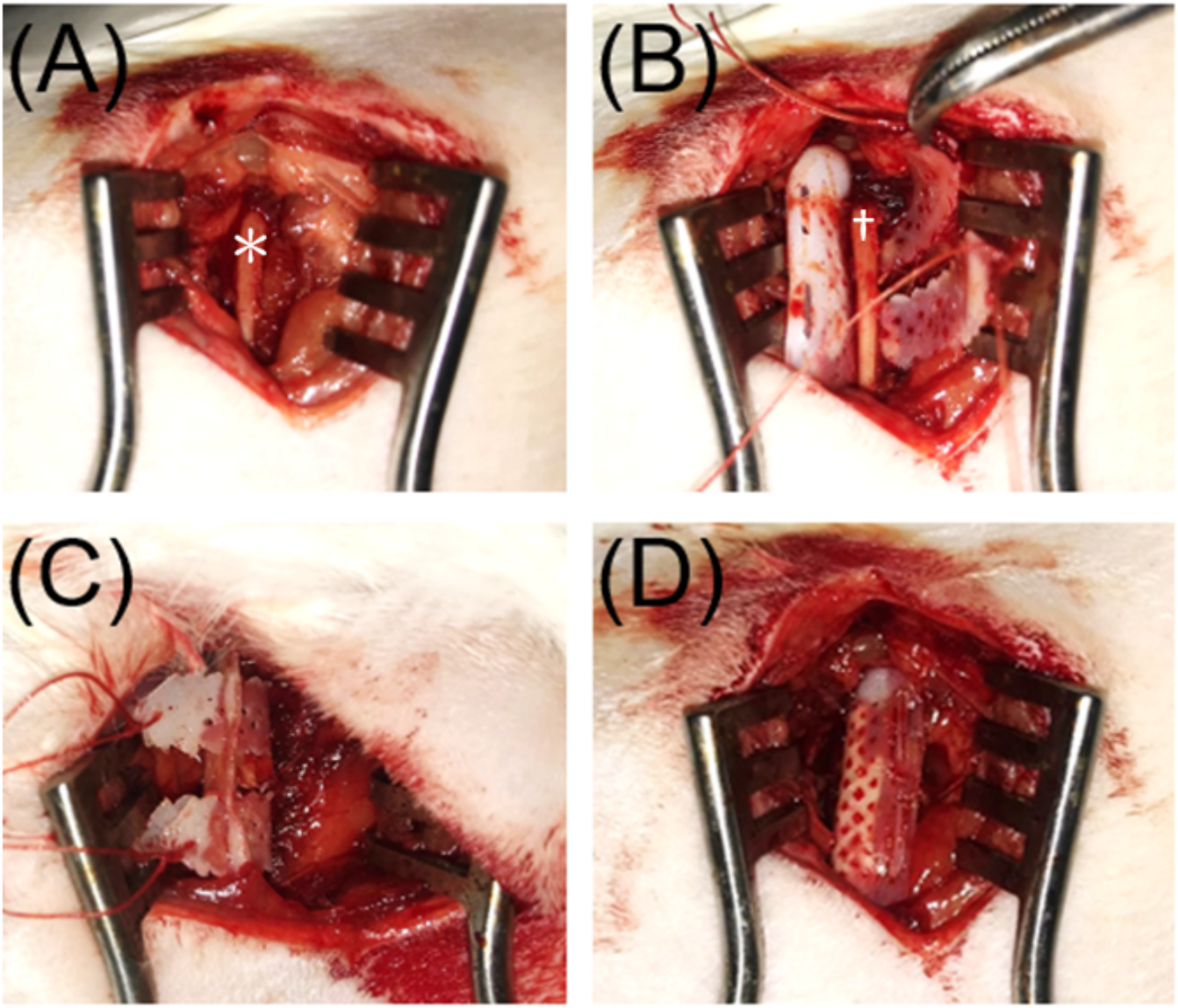

Figure 8

Rib-fracture model and implantation process. (A) The target rib (□) was reached after careful dissection of the soft tissue layer by layer. (B) An oblique fracture was created (†), and the hybrid fixator was placed underneath the osteotomized rib. (C) Belts were passed through matching holes and tightened. (D) The over-length belts were cut to smoothen the edges of the fixator.

Supplementary Files

This is a list of supplementary files associated with this preprint. Click to download.

- Graphicalabstract.png